Neutron-proton analyzing power measurements from 375 to 775 MeV

C. R. Newsom,* C. L. Hollas,† R. D. Ransome,‡ and P. J. Riley
University of Texas, Austin, Texas 78712

B. E. Bonner,§ J. G. J. Boissevain, J. J. Jarmer, M. W. McNaughton, and J. E. Simmons
Los Alamos National Laboratory, Los Alamos, New Mexico 87545

T. S. Bhatia,† G. Glass, J. C. Hiebert, L. C. Northcliffe, and W. B. Tippens**
Texas A&M University, College Station, Texas 77843
(Received 24 October 1988)

As part of an experimental study of the nucleon-nucleon interaction at medium energy, the free neutron-proton analyzing power $A_n(\theta_n^*, T_n)$ has been measured at nine incident neutron energies in the range $375 \leq T_n \leq 775$ MeV and for neutron c.m. angles in the range $57° \leq \theta_n^* \leq 159°$. Unpolarized neutrons with a broad continuum of energies, produced by interaction of an 800 MeV proton beam with a beryllium target, were scattered from a polarized proton target. At each angle, for the whole energy region, the scattered neutron and conjugate recoil proton were detected in coincidence. A previously unseen minimum is observed in the energy dependence of $A_n(\theta^* \sim 100°)$ near 625 MeV.

I. INTRODUCTION

Understanding of the isoscalar ($I=0$) part of the nuclear force at medium energies requires comprehensive measurements of neutron-proton (n-p) scattering observables, including those involving the spins and relative orbital angular momenta of the nucleons. Experimental activity in this field began more than 20 years ago,[1] although it was recognized much earlier that information on the noncentral nature of the nuclear force must be obtained through measurements of spin dependence. Nucleon-nucleon (N-N) phase-shift analyses (PSA's) combine the proton-proton (p-p) and n-p data in such a way that the $I=1$ phases are determined by the generally more accurate p-p data; the $I=0$ phases can only be determined after n-p experiments have been done.

The analyzing power is directly sensitive to those phase shifts which depend on spin-orbit terms. Analyzing power measurements in the medium-energy region will contribute to an understanding of the energy dependence of spin-orbit forces in the $I=0$ D and G waves. Measurements of the analyzing power are also of particular importance because the measurements of other spin observables almost always hinge upon knowledge of the analyzing power.

Most of the previous "n-p" data in the 500–800 MeV region were actually p-"n" data obtained by quasi-free proton-deuteron scattering.[2] The experiment reported here is a measurement of the *free* n-p analyzing power $A_n(\theta_n^*, T_n)$ for neutron c.m. angles $57° \leq \theta_n^* \leq 159°$ and laboratory energies $375 \leq T_n \leq 775$ MeV. In this experiment a neutron beam of large energy spread was collimated onto a polarized proton target, so that free n-p analyzing power data for a given angular range of about 16 deg in the center of mass were accumulated simultaneously for the wide region of neutron energies between 375 and 775 MeV. Since normalization errors caused by uncertainties in the target polarization were the same for all energies at each angle setting, the shape of the energy dependence of $A_n(\theta_n^*, T_n)$ at each angle was reliably determined in this experiment, since energy-dependent false asymmetries were considered to be negligible.

II. APPARATUS AND EXPERIMENTAL METHOD

The experiment was performed at the Clinton P. Anderson Meson Physics Facility (LAMPF) with the setup shown in Fig. 1. General aspects of the experimental method have been described earlier.[3,4] A summary is presented in the following, with emphasis on new elements.

A. Neutron beam

The LAMPF primary H^- beam (later stripped to become a proton beam) was of nominal energy, 800 MeV, and intensity 1–4 μA. It was tightly bunched by the 201.25 MHz acceleration voltage into very short micropulses (0.25 ns width) separated by $\sim$5 ns. The neutron beam was produced by passage of the protons through a beryllium target of 10 cm thickness. The neutron flux produced at 0° was collimated with a 2.54 cm diameter

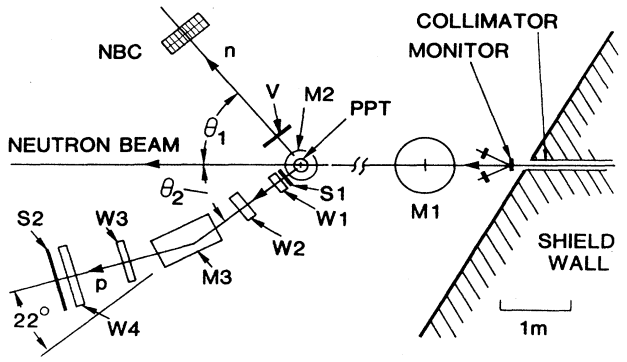

FIG. 1. Schematic plan view of the experimental setup.

hole in a steel insert of length 3.7 m contained in a thick concrete shield wall. The collimator exit was ~7 m downstream of the Be target. The proton beam was deflected through 60° and buried in a beam dump upstream of the shield wall. The shape of the neutron energy spectrum is shown in Fig. 2; it had a pronounced charge-exchange (CE) peak centered at neutron energy $T_n = 775$ MeV, as well as a broad distribution at lower energies, associated primarily with pion production in the Be target; the spectrum was cut off kinematically at ~100 MeV and instrumentally near 300 MeV. The width of the CE peak (~40 MeV) was caused primarily by the variation of energy loss in the Be target. A lead plug of thickness 3.8 cm was placed in the approximate center of the collimator, in order to substantially reduce the gamma-ray component of the beam.

B. Neutron beam monitor

The primary neutron intensity monitor was located immediately downstream of the collimator (see Fig. 1). It consisted of two symmetrically placed scintillator telescopes which viewed a polyethylene radiator located in the beam from left- and right-scattering angles of 25°. Charged particles in the beam were vetoed by an anticoincidence counter, placed upstream of the radiator. A magnet $M1$ located downstream of the monitor swept charged particles produced in the radiator (or anywhere else upstream of $M1$) out of the neutron beam.

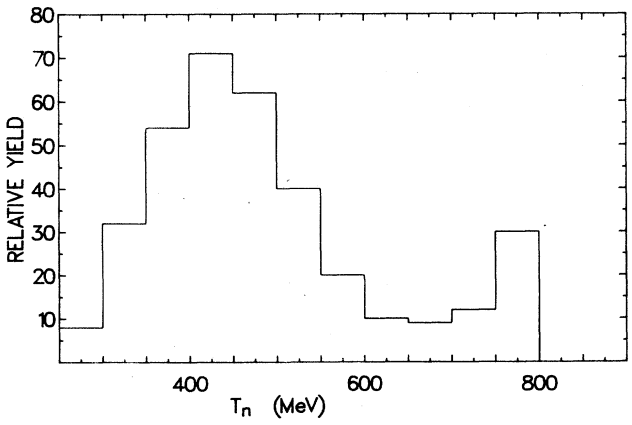

FIG. 2. Incident neutron energy spectrum.

C. Outline of the experiment

The neutron beam passed through a polarized proton target (PPT), and n-p elastic scattering in the target was detected by conjugate neutron and proton detectors. The scattered neutrons were detected in an array of scintillators labeled NBC (neutron bar counter), and the conjugate recoil protons were detected in a multiwire-proportional-chamber (MWPC) spectrometer system consisting of magnet $M3$, scintillators $S1$ and $S2$, and four MWPC's ($W1$–$W4$). The asymmetry was measured in the scattered yield upon reversal of the target polarization.

D. MWPC spectrometer

The MWPC spectrometer and its readout system were essentially the same as one described in detail in an earlier paper.[4] The one major difference was in the high-voltage planes of the MWPC's which were fabricated from aluminized Mylar instead of a grid of wires. Each MWPC had an x and a y plane with sense-wire spacing of 2 mm. The angle with which a particle emerged from the strong (2.5 T) field of the PPT magnet $M2$ was given by the coordinate information from $W1$ and $W2$, and the additional information from $W3$ and $W4$ gave the deflection of the particle by the field of the spectrometer magnet $M3$. From the observed angular deflection, a measurement of the particle momentum (with typical resolution $\Delta p/p \sim 0.02$) was obtained. The time of flight (TOF) between $S1$ and $S2$ could be used to determine the velocity of the particle, and thus its mass. The timings of the pulses from $S1$ and $S2$ (and all other scintillators in the experiment) were determined with constant-fraction discriminators (CFD's), and all timings were measured relative to the $S1$ CFD signal. Since the particle orbit is overdetermined by the data from four MWPC's, events were accepted whenever at least three of the four x and three of the four y planes showed hits, together with signals from $S1$ and $S2$. For each event the relative time difference t_{rf} between the $S1$ pulse and a pulse synchronized with the accelerator rf cycle was also measured, giving information on the incident neutron velocity. This parameter provided an independent measurement of the neutron energy, which was particularly helpful at lower incident energies, where it could be used to discriminate between events initiated by low-energy incident neutrons and those initiated by high-energy neutrons interacting inelastically in the PPT, the latter being the main source of background events.

E. Neutron detector

A valid coincident signal was required from the NBC. This detector was a scintillator hodoscope consisting of 18 rectangular bars made of NE110 arranged in two tandem banks of 9 bars each (long axis vertical). Each bar was 101 cm high, 7 cm wide, and 10.1 cm deep, and was viewed from each end, through acrylic light guides of length 22 cm, by Amperex XP2230 photomultiplier tube (PMT) assemblies. The vertical location of the interaction in a given bar could be determined with an accuracy ~ 5 cm (FWHM) by measurement of the time difference between the signals from the top and bottom PMT's of that bar; this was about the same as the horizontal resolution of 7 cm given by the width of the bar. The time average of the top and bottom signals gave the neutron TOF (measured relative to the signal from $S1$) with a time resolution ~ 1 ns. A veto scintillator plane (V) placed between the target and the NBC made it possible to reject charged particles in the trigger. Thus, the complete trigger signaling an acceptable event was

$$S1\cdot S2\cdot(W1_x\cdot W2_x\cdot W3_x\cdot W4_x)_{3/4}\cdot(W1_y\cdot W2_y\cdot W3_y\cdot W4_y)_{3/4}(\mathrm{NBC})\cdot\bar{V}\ .$$

Gains of the PMT's were equalized by use of a ^{60}Co source to set pulse-height thresholds near 1 MeV electron equivalent.

F. Polarized hydrogen target

The polarized target was developed for N-N experiments by a Los Alamos group headed by one of us (J.E.S.).[5] The target material consisted of propanediol ($C_3H_8O_2$) beads of diameter ~ 1 mm, doped by a well-known process[6] with 2% by weight of Cr^V complex. The target cavity was a sphere of diameter 4.57 cm, truncated symmetrically at top and bottom to have a vertical height of 2.79 cm. The volume of the cavity was ~ 40 cm^3. The estimated density of hydrogen was ~ 0.07 g/cm^3, resulting in ~ 2.9 moles of hydrogen. The target was located in a uniform 2.5 T vertical magnetic field, and was refrigerated to ~ 0.5 K by a ^{3}He refrigerator system precooled by liquid ^{4}He. Enhanced polarization was achieved by irradiating the material with ~ 69 GHz microwave radiation. The target polarization was monitored with a conventional parallel electrical circuit (LC) Q-meter nuclear magnetic resonance (NMR) system with dummy cell subtraction. The system was calibrated by measuring the signal size with the target in thermal equilibrium (TE) at 1 K (with the microwave power turned off). Under these conditions the target had a known polarization of $\sim 0.25\%$ calculated from the Boltzmann distribution of the spin-state populations. The gain of the amplifier in TE mode was increased by a factor of 50 over the enhanced mode. The TE temperature was determined with an accuracy of $\sim 0.1\%$ by measuring the ^{3}He vapor pressure with a commercial capacitance manometer. The measured enhanced polarization varied in the range 0.70 ± 0.02. The gain of the NMR system, as determined by the TE measurements, varied in time by as much as $\sim 0.45\%$ per day. This variation appeared as a drift over a period of 20 days of data accumulation. Since the calibration was checked only about once a week, it could not be ascertained that this variation was indeed a monotonic drift. Therefore it was treated solely as a contribution to the systematic error. The 9% overall variation was conservatively considered to contribute $\pm 6\%$ quadratically to the systematic error, and when combined with the other NMR calibration uncertainties it increased the systematic error by 3%. All errors here are percentages of the measured quantities (i.e., relative).

Changes between polarization states parallel and antiparallel to the applied field were achieved by altering the microwave frequency. This method avoided the systematic errors encountered by the field reversal technique, but since the order of ~ 30 min was required to reverse the polarization in this way, it was done only about three times a day.

G. p-p calibration

At the conclusion of the n-p running period, a p-p scattering calibration run was undertaken in order to verify the accuracy of the NMR measurements of target polarization. Setup of the experimental conditions was less than ideal because the beam profile could not be controlled. The neutron collimator was removed, and a proton beam of intensity < 1 pA was allowed to drift down the original neutron beam line; its diameter at the PPT was ~ 4 cm. Monitoring was chiefly accomplished by use of the left-right counter telescopes described above, but was supplemented by measurements made with an ion chamber placed in the beam. Magnet $M1$ was used as a steering magnet to compensate for the steering of the beam by the PPT magnet $M2$. The spectrometer and NBC array were interchanged and positioned so as to detect left-scattered protons at average c.m. angle $\theta_n^* = 60°$ in the NBC along with conjugate protons in the spectrometer. Counter V was used as a coincidence counter rather than a veto counter.

The standard NMR system was employed for measurement of the target polarization. Unfortunately, an accidental warmup of the target during the setup process melted the original target material, and new material had to be used. After this change, the TE response was 10% less than with the previous beads. Although the target sample was different, the NMR system and TE calibration procedure were the same, and this was considered to be a reasonable test of the system.

The p-p analyzing power value measured with this system turned out to be $\sim 4\%$ (relative) lower than the value found by Bevington *et al.*,[7] indicating that the NMR measurements of target polarization were too high by $\sim 4\%$. Thus, all measurements of the target polarization were reduced by the factor 0.961, and the estimated normalization error due to uncertainty of target polarization

was increased by 5% in quadrature, resulting in an overall target polarization uncertainty of ±7% (relative).

III. DATA ANALYSIS

The n-p elastic scattering signal was extracted from background by kinematic selection, over a range of incident neutron energies. In order to determine the true recoil angles of the proton at the target from the path observed in the spectrometer, it was necessary to correct for the deflection of the proton in the magnetic field of the PPT. Then, from the measurement of proton momentum provided by the spectrometer, with the assumption that the event was a n-p elastic scattering, the momentum of the scattered neutron was predicted, along with the horizontal (x) and vertical (y) coordinates expected for the neutron at the NBC and the time difference (t) expected between the $S1$ signal and the NBC signal. Histograms of the differences Δx, Δy, and Δt between the observed and predicted values of these parameters were constructed. Elastic n-p scattering produced a reasonably sharp peak in each of these histograms. The angular resolution of the apparatus ($\sim\pm 1.5°$ in the c.m. system) and the finite size of the target contributed to the widths of the Δx and Δy peaks. Software gates including only the peak regions in the Δx and Δt histograms were used to exclude much of the background in the generation of the Δy histogram. Since the off-peak Δy values reflect deviations from coplanarity of the reaction, the Δy histogram was taken as the fundamental signal. It contained a fairly sharp n-p elastic scattering peak superimposed upon a broad continuum attributed to quasi-free n-"p" scattering from target components other than hydrogen. Events associated with π^0 production also contributed to this continuum. A typical example is shown in Fig. 3.

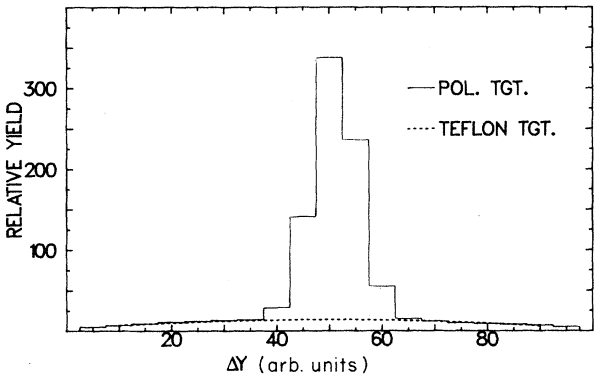

FIG. 3. Histogram of Δy, which shows the distribution of the deviation from coplanarity of the conjugate reaction products. The solid curve was obtained with the PPT and contains both elastic n-p and background events. The dotted curve was obtained with a Teflon target, which contains no hydrogen and simulates the contribution of background events; these are mostly attributed to quasi-free n-p scattering.

The kinetic energy T_n of the incident neutron could be determined in three ways: (1) from the proton angle and momentum, (2) from the neutron angle and proton momentum, and (3) from the $t_{\rm rf}$ signal, which reflected the neutron TOF over the 12.3 m flight path from the Be target to $S1$. In method (3), the "frame-overlap" ambiguity caused by faster neutrons from a given beam pulse overtaking and passing slower neutrons from earlier pulses was resolved by the measurements of methods (1) and (2). A weighted average of the three measurements was adopted as the T_n value. At the lower energies, the use of method (3) significantly improved the determination. The overall resolution of this determination was usually better than 30 MeV (FWHM).

For each spectrometer setting, the Δy histograms (separately for positive and negative target polarizations) were sorted into nine energy bins, each 50 MeV wide, and into 3 or 4 c.m. angle bins. A least-squares fit in which the signal was represented by a Gaussian curve and the background by a quadratic function was made for each Δy histogram. As a result, any effect due to an asymmetry in the background was eliminated automatically. The signal to background ratio varied from 3 to 20, with a typical value of 10. Live time and neutron monitor normalizing factors were used to obtain the relative signal intensities $I(\pm)$ for each histogram, where + or − indicates the direction up or down of proton target polarization. The scattering asymmetries

$$\epsilon=\frac{I(+)-I(-)}{I(+)+I(-)} \tag{1}$$

were then calculated for each (T_n,θ_n^*) bin, and the n-p analyzing power was obtained for each bin through the formula

$$A_n(\theta_n^*,T_n)=\frac{\epsilon}{P+\epsilon\Delta P}\ , \tag{2}$$

where P is the average magnitude of (+) and (−) target polarizations and ΔP is the difference between these; ΔP was seldom greater than 0.03 in magnitude.

Differences in beam intensity for the two target polarization states lead to dead-time effects for which a correction was made based on a small correlation observed between individual measurements of A_n at different beam intensities. The maximum correction was 5% ± 3.5% (relative).

IV. RESULTS

The measured analyzing power values $A_n(\theta_n^*,T_n)$ are presented in Fig. 4 and numerically in Table I. As noted earlier, the "white spectrum" of incident neutrons has been divided into nine kinetic energy bins, each of 50 MeV width, the central energy being indicated for each bin. The errors shown are statistical only. Superimposed on these should be a systematic uncertainty estimated to be ~7%, arising from uncertainty in the target polarization measurements mentioned earlier. This last error reflects possible variations in the calibration at different angle settings.

Also shown in Fig. 4 are the predictions (or fits) of several phase-shift analyses (PSA's). All of these were obtained using the computer code SAID of Arndt *et al.*[8] with a recently updated database. This database contains as yet unpublished data[9] which are not presented here. The curves labeled FA87 are given by the energy-dependent PSA of Arndt *et al.*, while those labeled C400–C800 are extrapolations from their "single-energy" fits at 400, 500, 600, 700, and 800 MeV. The curves labeled SACL are those given by the energy-dependent PSA of the Saclay group.[1] The data of this experiment were included in the database for all of the above-mentioned PSA's, but not in the database for two older PSA's, that of the BASQUE group[10] labeled BASQ, and that of Hoshizaki[11] labeled HOSH. As would be expected, the PSA's of Refs. 10 and 11 do not fit the data of this experiment nearly as well as do the PSA's of Refs. 1 and 8. Overall, the SACL fits seem to be the best.

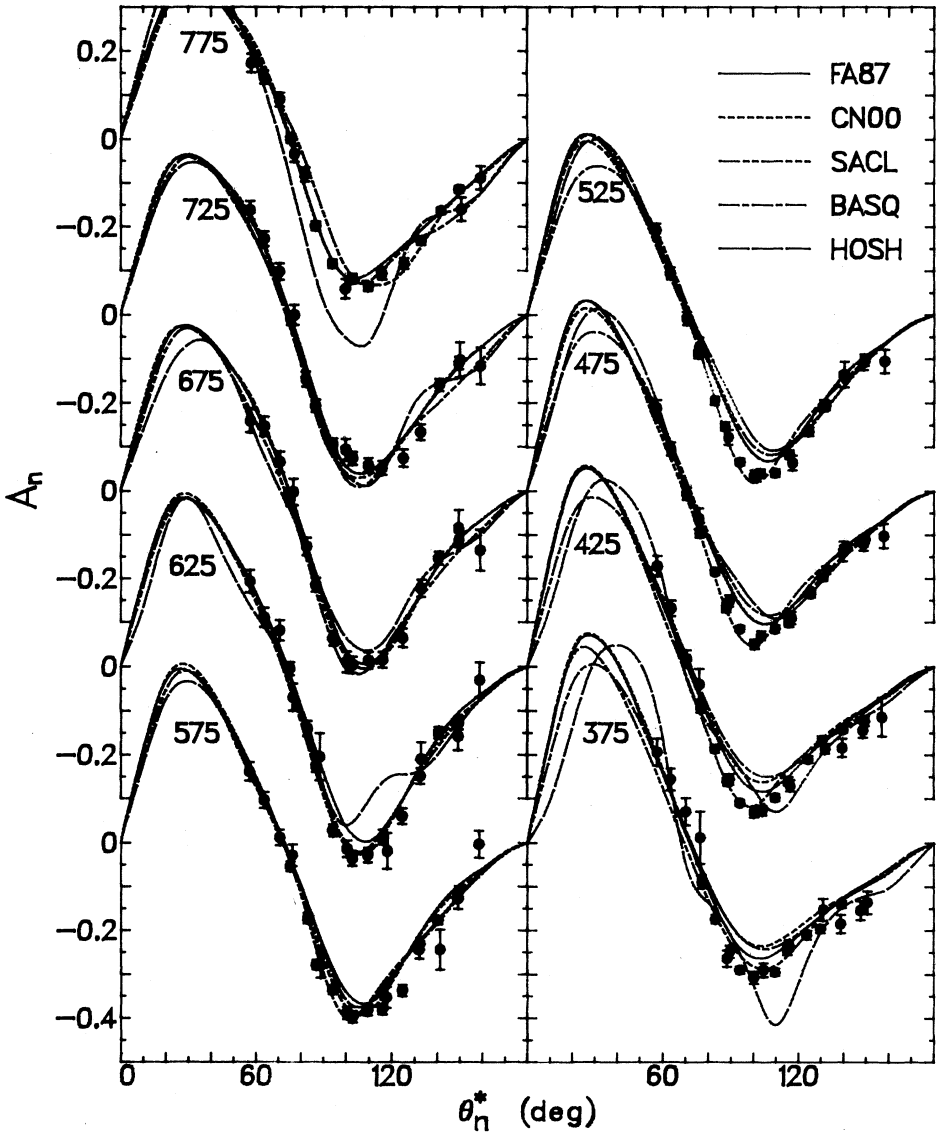

FIG. 4. Comparison of the results of this experiment with various PSA fits (or predictions). The data have been sorted into incident neutron energy bins of width 50 MeV. The central energy (in MeV) is indicated for each bin. The curves labeled FA87 and N00 are the energy-dependent and single-energy fits of Arndt *et al.* (Ref. 8), respectively, where N00 signifies the energy of the nearest single-energy fit of Ref. 8. Those labeled SACL are the energy-dependent fits of the Saclay group (Ref. 1). The curves labeled BASQ and HOSH are the predictions of the BASQUE group (Ref. 10) and Hoshizaki (Ref. 11), respectively. The errors shown here and in all subsequent figures are statistical only. Refer to the text for a discussion of the systematic errors, which are *not* purely normalization uncertainties.

TABLE I. Experimental analyzing power values. The stated errors are statistical only and do not reflect the systematic error, which is *not* in normalization only. See the text for an explanation of the systematic error.

T_n (MeV)	θ_n^* (deg)	$A(\theta_n^*)$	T_n (MeV)	θ_n^* (deg)	$A(\theta_n^*)$	T_n (MeV)	θ_n^* (deg)	$A(\theta_n^*)$
375	57.6	0.206±0.031	425	57.6	0.229±0.023	475	57.2	0.189±0.018
	63.6	0.144±0.025		63.7	0.132±0.018		63.6	0.096±0.015
	70.2	0.071±0.031		70.4	0.018±0.019		70.6	−0.006±0.014
	76.5	0.012±0.060		76.1	−0.040±0.035		75.8	−0.063±0.024
	77.1	−0.089±0.015		76.7	−0.092±0.012		76.2	−0.096±0.010
	83.1	−0.175±0.010		83.0	−0.187±0.009		82.9	−0.185±0.008
	88.3	−0.264±0.019		88.4	−0.258±0.013		87.9	−0.267±0.010
	89.5	−0.248±0.014		89.4	−0.256±0.012		89.2	−0.251±0.013
	94.1	−0.290±0.008		94.0	−0.309±0.007		94.0	−0.315±0.007
	100.1	−0.308±0.014		100.2	−0.330±0.012		100.4	−0.350±0.011
	104.5	−0.290±0.016		103.9	−0.326±0.011		103.4	−0.330±0.010
	109.7	−0.295±0.008		109.7	−0.297±0.008		109.7	−0.315±0.008
	115.1	−0.244±0.012		115.4	−0.260±0.010		115.7	−0.301±0.009
	115.7	−0.234±0.012		116.3	−0.270±0.013		116.8	−0.290±0.014
	123.7	−0.210±0.010		124.3	−0.210±0.008		125.4	−0.235±0.008
	129.8	−0.196±0.009		130.4	−0.166±0.010		130.8	−0.195±0.010
	130.9	−0.152±0.025		131.9	−0.186±0.011		132.3	−0.180±0.009
	138.7	−0.185±0.021		139.4	−0.184±0.021		139.8	−0.137±0.023
	139.1	−0.140±0.008		139.8	−0.142±0.007		140.1	−0.131±0.007
	147.5	−0.154±0.022		148.5	−0.144±0.017		148.8	−0.120±0.016
	150.5	−0.136±0.026		149.3	−0.123±0.011		149.4	−0.108±0.009
				156.9	−0.114±0.044		157.7	−0.102±0.028
525	57.1	0.192±0.016	575	57.1	0.162±0.021	625	57.2	0.194±0.026
	63.5	0.094±0.014		63.6	0.097±0.018		63.6	0.111±0.022
	70.6	−0.008±0.015		70.6	0.012±0.018		70.6	0.082±0.023
	75.6	−0.089±0.010		75.3	−0.054±0.011		75.1	−0.005±0.015
	76.0	−0.073±0.022		76.2	−0.029±0.025		76.4	−0.069±0.031
	82.9	−0.195±0.010		82.9	−0.173±0.012		82.8	−0.141±0.017
	87.4	−0.253±0.010		86.9	−0.279±0.011		86.7	−0.226±0.014
	88.9	−0.278±0.017		88.7	−0.281±0.028		88.3	−0.205±0.054
	94.0	−0.334±0.008		94.0	−0.336±0.010		94.1	−0.372±0.014
	100.5	−0.364±0.011		100.5	−0.389±0.014		100.4	−0.414±0.019
	103.1	−0.360±0.010		102.9	−0.398±0.013		102.7	−0.436±0.017
	109.6	−0.359±0.009		109.6	−0.382±0.012		109.6	−0.428±0.017
	115.9	−0.317±0.010		116.0	−0.380±0.012		116.0	−0.387±0.017
	117.3	−0.336±0.017		117.8	−0.353±0.024		118.0	−0.419±0.041
	124.6	−0.264±0.010		124.7	−0.337±0.013		124.7	−0.339±0.018
	131.3	−0.205±0.013		132.1	−0.244±0.020		132.6	−0.248±0.018
	132.2	−0.205±0.010		132.5	−0.230±0.014		132.9	−0.209±0.038
	140.3	−0.135±0.007		140.4	−0.177±0.009		140.5	−0.149±0.013
	140.4	−0.135±0.029		141.3	−0.244±0.046		149.3	−0.158±0.032
	149.0	−0.107±0.018		149.2	−0.128±0.023		149.5	−0.127±0.015
	149.3	−0.105±0.010		149.5	−0.111±0.012		158.8	−0.030±0.040
	158.2	−0.105±0.027		158.6	−0.003±0.031			
675	57.3	0.160±0.027	725	57.4	0.238±0.021	775	57.9	0.173±0.021
	63.6	0.147±0.022		63.6	0.172±0.017		63.6	0.141±0.015
	70.6	0.066±0.024		70.5	0.098±0.019		70.5	0.090±0.016
	75.1	−0.018±0.017		75.3	−0.009±0.014		75.3	0.002±0.011
	76.6	−0.002±0.030		77.0	0.000±0.023		77.0	−0.033±0.019
	82.5	−0.127±0.020		82.1	−0.146±0.017		81.7	−0.081±0.016
	86.5	−0.215±0.016		86.4	−0.207±0.014		86.4	−0.199±0.010
	94.1	−0.337±0.016		94.1	−0.295±0.014		93.9	−0.284±0.010
	100.1	−0.390±0.024		99.8	−0.306±0.024		99.6	−0.341±0.022
	102.7	−0.397±0.019		102.7	−0.326±0.015		102.7	−0.318±0.011
	109.7	−0.386±0.019		109.6	−0.341±0.016		109.6	−0.336±0.010
	115.9	−0.385±0.018		115.7	−0.348±0.016		115.7	−0.306±0.014

TABLE I. (*Continued*).

T_n (MeV)	θ_n^* (deg)	$A(\theta_n^*)$	T_n (MeV)	θ_n^* (deg)	$A(\theta_n^*)$	T_n (MeV)	θ_n^* (deg)	$A(\theta_n^*)$
	124.8	−0.335±0.021		125.1	−0.325±0.020		125.5	−0.283±0.012
	132.9	−0.222±0.020		132.8	−0.266±0.018		133.0	−0.231±0.010
	140.7	−0.153±0.015		141.0	−0.159±0.014		141.8	−0.163±0.008
	149.5	−0.084±0.041		149.7	−0.109±0.014		149.8	−0.114±0.008
	149.6	−0.111±0.017		150.1	−0.102±0.040		150.8	−0.160±0.027
	159.1	−0.135±0.047		159.2	−0.116±0.042		159.3	−0.088±0.027

In Fig. 5 the data of this experiment are compared with most of the data[2,12–25] included in the SAID database. Omitted are some measurements by Sakuda *et al.*[26] and Kazarinov *et al.*,[27] which have very large error bars and, for the most part, are not in disagreement with the results of this experiment. Since the only published results available between 650 and 700 MeV are those of Sakuda *et al.*, the 675 MeV results are not displayed in Fig. 5.

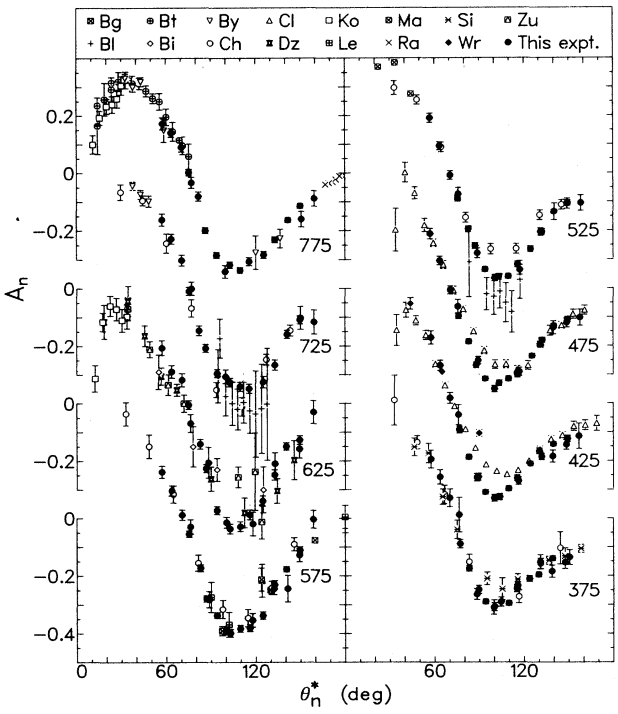

FIG. 5. Comparison of the results of this experiment with other available data at comparable energies. The labels are as follows: Ba—Bagaturia *et al.*, 600 MeV (Ref. 12); Bl—Ball *et al.*, 544 and 719 MeV (Ref. 13); Bt—Barlett *et al.*, 800 MeV (Ref. 14); Bi—Bilenkaya *et al.*, 605 MeV (Ref. 15); By—Bystricky *et al.*, 725 and 800 MeV (Ref. 16); Ch—Cheng *et al.*, 400, 500, 600, and 700 MeV (Ref. 2); Cl—Clough *et al.*, 425 and 495 MeV (Ref. 17); Dz—Dzhelepov *et al.*, 635 MeV (Ref. 18); Ko—Korolev *et al.*, 633 and 784 MeV (Ref. 19); Le—Leung, 600 MeV (Ref. 20); Ma—Marshall *et al.*, 500 MeV (Ref. 21); Ra—Ransome *et al.*, 790 MeV (Ref. 22); Si—Siegel *et al.*, 350 MeV (Ref. 23); Wr—Wright *et al.*, 425 MeV (Ref. 24); Zu—Zulkarneev *et al.*, 635 MeV (Ref. 25).

A common feature shared by all of these angular distributions is the existence of a positive maximum for A_n at angles near 30° and a minimum (negative maximum) for angles near 100°. The minimum is much better determined experimentally than the maximum. The results of this experiment are in good agreement with most of the data except in the vicinity of this minimum, where no simple pattern of discrepancy is apparent. For example, there is good agreement with the 400 and 600 MeV data of Cheng *et al.*[2] (shown at 375 and 575 MeV in Fig. 5), while Cheng *et al.* find a shallower minimum at 500 MeV (shown at 525 MeV) and a deeper minimum at 700 MeV (shown at 725 MeV). On the other hand, Ball *et al.*[13] find a deeper minimum at 544 MeV (compared at 525 MeV) and also at 719 MeV (compared at 725 MeV). Recent measurements[28] at 744 and 794 MeV tend to confirm the results of the present experiment, although not with high statistical precision. In order to reduce the clutter, these results are not shown in Fig. 5.

The biggest disagreement appears to be with the statistically precise measurements of Clough *et al.*[17] at 425 and 495 MeV, where they find the minimum to be shallower. The source of this disagreement is not understood, especially since the A_n values obtained in the present experiment are in agreement with those of Cheng *et al.*[2] at all energies except 525 MeV, and the values of Ref. 2 were used (in part) by Clough *et al.* in normalization of their data. More specifically, Clough *et al.*[17] normalized their A_n values (via PSA) using two kinds of input: (a) the absolute A_n values measured by Cheng *et al.*[2] (and at lower energies by Tinlot and Warner[29]); (b) the measured polarization-transfer parameter R_t for free n-p scattering and r for quasi-free p-n scattering from deuterium, corrected for three-body effects (in the notation of Ref. 17 in which the exact procedure is described). The two normalizations they obtained differed by only 3%, and the one they adopted was the average of the two. Thus, the A_n values of Clough *et al.* should be in reasonable agreement with Cheng *et al.* in the 300–500 MeV energy region. As can be seen from Fig. 5, however, the A_n values of the present experiment are in good agreement with those of Cheng *et al.* at all energies except 525 MeV, but are in sharp conflict with Clough *et al.* in the region 400–500 MeV. We see no way of resolving this difficulty. It should be noted, however, that at 400 MeV there are no data from Cheng *et al.* in the angular region where the results of the present experiment disagree substantially with those of Clough *et al.*

It is not possible to attribute these disagreements to the normalization uncertainty in this experiment, because that comes from the uncertainty of the target polarization and is the *same for all energies* at a given angle, while the disagreements are different for different energies. Of particular interest is the variation with energy of the minimum in A_n, which occurs near $\theta_n^* = 100°$. A plot of the values of $A_n(\theta_n^* = 100°)$ vs T_n found in this experiment, several other experiments,[2,13–27,29–32] and the PSA's is presented in Fig. 6. The values of $A(100°)$ for this experiment were obtained with second-order least-squares fits to points in the vicinity of 100° (80°–118°), whereas the values for other experiments were chosen from their direct measurements in the range 97°–102°. The error bars shown on the graph are indicative of the statistical error of the points in this region. Incidentally, it was found that Legendre polynomial fits to the entire angular range of the present experiment yielded a smoother energy dependence in the region 625–775 MeV. It was felt, however, that the local fits were more representative of these data in the vicinity of the minima. It is evident (especially from the results of this experiment) that the back-angle n-p analyzing power $A(\sim 100°)$ goes through a minimum value near 625 MeV. The previous experiments (especially that of Cheng *et al.*[2]) showed a monotonic decrease of $A(\sim 100°)$ up to 700 MeV and did not reveal the existence of a minimum, although they were not inconsistent with it. While no specific explanation is advanced for the existence of this minimum, it is worth noting that a similar minimum is seen in the analyzing power for p-p elastic scattering.

The angle at which the analyzing power passes through zero (the zero-crossing angle) is of interest to those engaged in tests of charge symmetry[33] and time reversal invariance,[34] because the absolute calibration of a polarimeter (in the case of time reversal tests) and the absolute measurement of polarization of beam or target are not necessary if the measurements are performed to determine the zero-crossing angle. Various charge-symmetry-breaking models[35] predict a difference in this angle for a polarized proton target as opposed to a polarized neutron beam. The observed energy dependence of this zero-crossing angle and some PSA predictions of it are shown in Fig. 7.

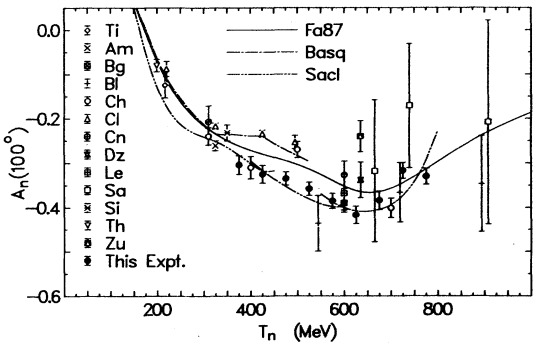

FIG. 6. Values of A_n vs T_n for $\theta_n^* = 100°$ (the most negative region of the angular distribution for A_n) as given by other experiments, various PSA's and the present experiment. The two-letter designation of other experimental points is the same as in Fig. 5, except as follows: Ti—Tinlot *et al.* (Ref. 29); Am—Amsler *et al.* (Ref. 30); Cn—Chamberlain *et al.* (Ref. 31); Sa—Sakuda *et al.* (Ref. 26); Th—Thomas *et al.* (Ref. 32). Note also that the symbols for Ti, Cn, Sa, and Th here are those used for Bi, Bt, Ko, and By, respectively, in Fig. 5. Also shown are the predictions of three PSA's, identified in the same way as in Fig. 4. The PSA prediction of Hoshizaki (Ref. 11) is not shown because it differs drastically from the data.

Another insight to be gained from these data is made possible by the separability of the $I=0$ and $I=1$ contributions to the quantity $A\,d\sigma/d\Omega$, which may be called the "spin-dependent cross section" since it combines both the analyzing power A and the differential cross section $d\sigma/d\Omega$ into a single quantity. In the formalism of MacGregor *et al.*,[36] with the assumption of time reversal invariance that A equals the polarization function P, the spin-dependent cross section for n-p scattering can be shown to be

$$P(n\text{-}p)\frac{d\sigma}{d\Omega}(n\text{-}p) = P^0(n\text{-}p)\frac{d\sigma}{d\Omega}(n\text{-}p) + P^1(p\text{-}p)\frac{d\sigma}{d\Omega}(p\text{-}p) + P^{01}(n\text{-}p)\frac{d\sigma}{d\Omega}(n\text{-}p)\,, \tag{3}$$

where the superscripts indicate the isospin state, and $P^{01}(n\text{-}p)$ is a term containing interference between $I=0$ and $I=1$ amplitudes. From the symmetry properties of these amplitudes, the pure isospin terms (the first and second terms on the right) are antisymmetric about 90°, while the interference (third term) term is symmetric. The equation can be rearranged to put experimentally determinable quantities on the left-hand side:

$$P(n\text{-}p)\frac{d\sigma}{d\Omega}(n\text{-}p) - P^1(p\text{-}p)\frac{d\sigma}{d\Omega}(p\text{-}p) = P^0(n\text{-}p)\frac{d\sigma}{d\Omega}(n\text{-}p) + P^{01}(n\text{-}p)\frac{d\sigma}{d\Omega}(n\text{-}p)\,. \tag{4}$$

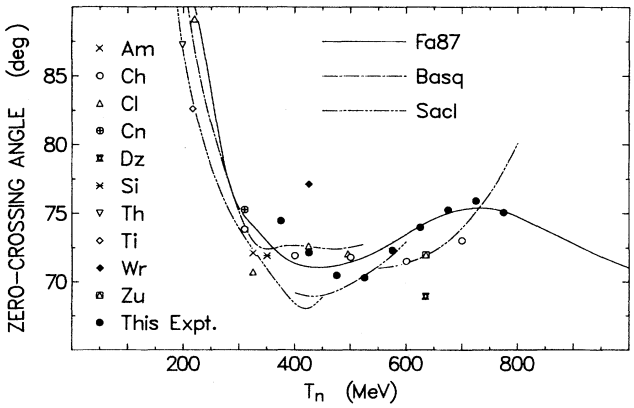

FIG. 7. Zero-crossing angle as a function of energy as given by this experiment, other experiments, and various PSA's. The two letter designation of the points is the same as in Figs. 5 and 6. Since only the trend of the data was meant to be seen here, the errors are not shown; for the data of the present experiment they are ~1°–2°.

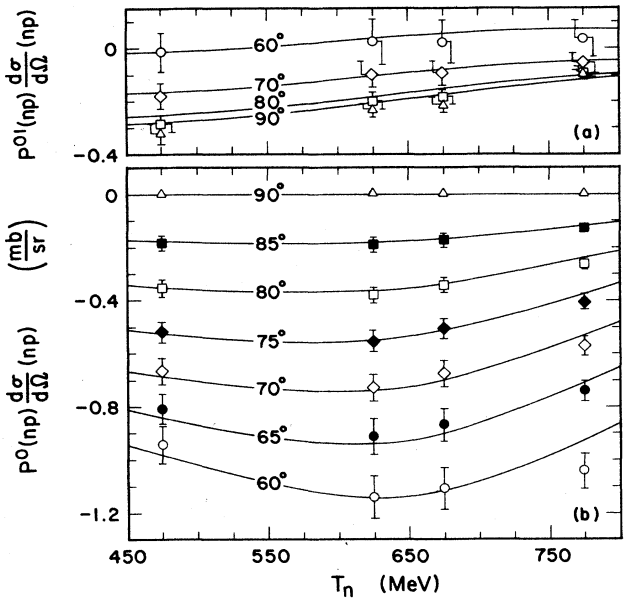

FIG. 8. (a) Interference contribution to the spin-dependent cross section versus energy at several angles. (b) Pure $I=0$ contribution versus energy at several angles. The errors shown are rough estimates based on the errors associated with the fits to both the analyzing power and the cross section data.

Since data are available for angles both below and above 90°, this side of the equation can be evaluated and broken up into symmetric and antisymmetric parts, which then determines the interference term (symmetric) and the pure $I=0$ term (antisymmetric) on the right-hand side.

The existence of extensive n-p differential cross section data at 459 MeV (Ref. 37), 647 MeV (Ref. 38), and 802 MeV (Ref. 39) makes it possible to carry out this procedure without too much extrapolation at four energies of this experiment (475, 625, 675, and 775 MeV). Fourth-order polynomials were fit to the $d\sigma/d\Omega(n\text{-}p)$ data[37–39] and to the data of the present experiment, so as to obtain smoothed values of these observables at 5° intervals of θ_n^*. The values used for $d\sigma/d\Omega(p\text{-}p)$ and $P^1(p\text{-}p)$ were those provided by the C450, C650, and C800 single-energy fits given by the PSA of Arndt *et al.*[8] at the same angles. The left-hand side of Eq. (4) was then evaluated at angles symmetric about 90° and broken into antisymmetric and symmetric parts. The results are presented in Figs. 8(a) and (b), which show, respectively, the interference (symmetric) and $I=0$ (antisymmetric) contributions to the "spin-dependent cross sections," as functions of incident neutron energy for a number of different angles. While the energy dependences seen in Fig. 8 are relatively structureless, the points are widely separated and it would be useful to have additional points at intermediate energies such as 525, 575, and 725 MeV. More cross section data in finer energy steps must become available in those regions to fill in these points.

The results presented here are measurements of an essential parameter describing free n-p elastic scattering. They also are necessary for the extraction of other spin-dependent parameters for n-p scattering experiments in this energy region.[22,33,34,40] Furthermore, these results have been employed in several PSA's and have contributed significantly to the building of the firm database required for the representation and understanding of the $I=0$ N-N interaction at medium energies.

ACKNOWLEDGMENTS

The efforts of LAMPF personnel at the Los Alamos National Laboratory are much appreciated; this experiment relied heavily on their expertise and assistance. We also thank Louis Rosen, the former director of LAMPF, for his strong encouragement of the nucleon-nucleon program. This work was supported in part by the United States Department of Energy, under Contract DE-AS05-76ER04449 and Grant DE-FG05-88ER40399.

*Present address: University of Iowa, Iowa City, IA 52242.
†Present address: Los Alamos National Laboratory, Los Alamos, NM 87545.
‡Present address: Rutgers University, New Brunswick, NJ 08903.
§Present address: Rice University, Houston, TX 77005.
**Present address: University of Virginia, Charlottesville, VA 22901.

[1]Reference to most of the earlier n-p data may be found in J. Bystricky and F. Lehar, *Physik Daten 11-1,* edited by H. Behrens and G. Ebel (Fachinformationszentrum, Karlsruhe, 1978), Parts 1 and 2; *Physik Daten 11-2 and 11-3,* edited by H. Behrens and G. Ebel (Fachinformationszentrum, Karlsruhe, 1981); see also J. Bystricky, C. Lechanoine-Leluc, and F. Lehar, J. Phys. (Paris) **48**, 199 (1987).
[2]D. Cheng, B. MacDonald, J. A. Helland, and P. M. Ogden, Phys. Rev. **163**, 1470 (1967).
[3]G. Glass, M. Jain, M. L. Evans, J. C. Hiebert, L. C. Northcliffe, B. E. Bonner, J. E. Simmons, C. Bjork, P. Riley, and C. Cassapakis, Phys. Rev. D **15**, 36 (1977).
[4]C. G. Cassapakis *et al.,* Phys. Lett. **63B**, 35 (1976); M. L. Evans *et al.,* Phys. Rev. C **26**, 2525 (1982).
[5]M. W. McNaughton *et al.,* Phys. Rev. C **23**, 838 (1981).
[6]W. de Boer, Nucl. Instrum. Methods **107**, 99 (1972).
[7]P. R. Bevington *et al.,* Phys. Rev. Lett. **41**, 384 (1978).
[8]R. A. Arndt, J. S. Hyslop III, and L. D. Roper, Phys. Rev. D **35**, 128 (1987); R. A. Arndt, L. D. Roper, R. A. Bryan, R. C. Clark, B. J. VerWest, and P. Signell, *ibid.* **28**, 97 (1983).
[9]T. S. Bhatia *et al.,* in *Polarization Phenomena in Nuclear Physics—1980 (Fifth International Symposium, Santa Fe),* Proceedings of the Fifth International Symposium on Polarization Phenomenon in Nuclear Physics, AIP Conf. Proc. No. 69, edited by G. G. Olsen, R. E. Brown, N. Jarmie, W. W. McNaughton, and G. M. Hale (AIP, New York, 1981), p. 123. The data for this experiment have been included in the database of Ref. 8 and will appear in a later publication.

[10]R. Dubois, D. Axen, R. Keller, M. Comyn, G. A. Ludgate, J. R. Richardson, N. M. Stewart, A. S. Clough, D. V. Bugg, and J. A. Edgington, Nucl. Phys. **A377**, 554 (1982).
[11]N. Hoshizaki, Prog. Theor. Phys. **60**, 1796 (1978); **61**, 129 (1979).
[12]Yu. Sh. Bagaturia *et al.*, Yad. Phys. **33**, 1237 (1981) [Sov. J. Nucl. Phys. **33**, 659 (1981)].
[13]J. Ball, V. Ghazikhanian, J. Gordon, F. Lehar, A. DeLesquen, F. Perrot, and L. van Rossum, Nucl. Phys. **B286**, 635 (1987).
[14]M. L. Barlett *et al.*, Phys. Rev. C **27**, 682 (1983).
[15]S. I. Bilenkaya, L. N. Glonti, Yu. M. Kazarinov, and V. S. Kiselev, Zh. Eksp. Teor. Fiz. **59**, 1049 (1970) [Sov. Phys.—JETP **32**, 569 (1971)].
[16]J. Bystricky *et al.*, Nucl. Phys. **A444**, 597 (1985).
[17]A. S. Clough *et al.*, Phys. Rev. C **21**, 988 (1980).
[18]V. P. Dzhelepov, Proceedings of the XII International Conference, Dubna, 1964 (unpublished).
[19]G. A. Korolev, A. V. Khanzadeev, G. E. Petrov, E. M. Spiridenkov, A. A. Vorobyov, Y. Terrien, J. C. Lugol, J. Saudinos, B. H. Silverman, and F. Wellers, Phys. Lett. **165B**, 262 (1985).
[20]K. C. Leung, made available by private communication in the databases of Refs. 1 and 8.
[21]J. A. Marshall, M. L. Barlett, R. W. Fergerson, G. W. Hoffmann, E. C. Milner, L. Ray, J. F. Amann, B. E. Bonner, and J. B. McClelland, Phys. Rev. C **34**, 1433 (1986).
[22]R. D. Ransome *et al.*, Phys. Rev. Lett. **48**, 781 (1982).
[23]R. T. Siegel *et al.*, Phys. Rev. **101**, 838 (1955).
[24]S. C. Wright, D. Shawhan, L. Pondrom, S. Olsen, and R. Handler, Phys. Rev. **175**, 1794 (1968).
[25]R. Zulkarneev, K. H. Murtazaev, and V. Khachaturov, Phys. Lett. **61B**, 164 (1976).
[26]M. Sakuda *et al.*, Phys. Rev. D **25**, 2004 (1982).
[27]Yu. M. Kazarinov *et al.*, Yad. Fiz. **4**, 567 (1966) [Sov. J. Nucl. Phys. **4**, 402 (1967)].
[28]A. de Lesquen *et al.*, Nucl. Phys. **B304**, 673 (1988).
[29]J. Tinlot and R. E. Warner, Phys. Rev. **124**, 890 (1961).
[30]C. Amsler *et al.*, Phys. Lett. **69B**, 419 (1977).
[31]O. Chamberlain, E. Segre, R. D. Tripp, C. Wiegand, and T. Ypsilantis, Phys. Rev. **105**, 288 (1957).
[32]A. R. Thomas, D. Spalding, and E. H. Thorndike, Phys. Rev. **167**, 1240 (1968).
[33]T. S. Bhatia *et al.*, Phys. Rev. C **24**, 796 (1981); S. E. Vigdor *et al.*, in *Polarization Phenomena in Nuclear Physics—1980* (Fifth International Symposium, Santa Fe), Proceedings of the Fifth International Symposium on Polarization Phenomenon in Nuclear Physics, AIP Conf. Proc. No. 69, edited by G. G. Olsen, R. E. Brown, N. Jarmie, W. W. McNaughton, and G. M. Hale (AIP, New York, 1981), p. 1455; R. Abegg *et al.*, Phys. Rev. Lett. **56**, 257 (1986).
[34]T. S. Bhatia *et al.*, Phys. Rev. Lett. **48**, 227 (1982).
[35]C. Y. Cheung, E. M. Henley, and G. A. Miller, Nucl. Phys. **A305**, 342 (1978); **A348**, 365 (1980); A. Gersten, Phys. Rev. C **18**, 2252 (1978); G. A. Miller, A. W. Thomas, and A. G. Williams, Phys. Rev. Lett. **56**, 2567 (1986); M. Beyer and A. G. Williams, Phys. Rev. C **38**, 779 (1988).
[36]M. H. MacGregor, M. J. Moravschik, and H. P. Stapp, Annu. Rev. Nucl. Sci. **10**, 291 (1960).
[37]Phys. Rev. C (to be published); the data are available in the database of SAID (see Ref. 8).
[38]M. L. Evans *et al.*, Phys. Rev. C **26**, 2525 (1982).
[39]M. Jain *et al.*, Phys. Rev. C **30**, 566 (1984).
[40]P. J. Riley *et al.*, Phys. Lett. **103B**, 313 (1981); J. Chalmers *et al.*, *ibid.* **153B**, 235 (1985); G. R. Burleson *et al.*, Phys. Rev. Lett. **59**, 1645 (1988).